Western Pacific Jet Stream Anomalies at 200 hPa in Winter Associated with Oceanic Surface Heating and Transient Eddy Activity*

REN Xuejuan†(任雪娟) and ZHANG Yaocun (张耀存)

Institute of Severe Weather and Climate, Department of Atmospheric Sciences, Nanjing University, Nanjing 210093

(Received April 12, 2007)

ABSTRACT

The relationships between the 200-hPa westerly jet stream anomalies over the East Asian coastal water-western Pacific (WPJS), and the oceanic surface heating and synoptic-scale transient eddy (STE) activity anomalies over the North Pacific in wintertime are examined by using ERA-40 and NCEP/NCAR reanalysis data. The analysis demonstrates that the surface heating and the STE anomalies have different patterns, corresponding to the three WPJS anomalous modes, respectively. In the first WPJS anomalous mode, the WPJS main part shows no robust anomaly. The anomalous westerly wind, occurring over the mid-latitude central-eastern Pacific past the date line is associated with the anomalous heating presenting both in the tropical central-eastern Pacific past the date line and the center of the North Pacific basin. Meanwhile, the STE anomaly appears around the region of the anomalous zonal wind. The fluctuation in jet strength shown in the second WPJS mode is strongly related to the heating anomaly in the Kuroshio Current region and the STE anomaly in the jet exit region. The third mode demonstrates a northward/southward shift of the WPJS, which has a statistical connection with a south-north dipolar pattern of the heating anomaly in the western North Pacific separated at 35°N. Meanwhile, the STE spatial displacement is in conjunction with jet shifts in the same direction. The heating anomaly has a close connection with the atmospheric circulation, and thus changes the mid-latitude baroclinicity, leading to the STE anomaly, which then reinforces the WPJS anomaly via internal atmospheric dynamics.

Key words: 200-hPa westerly jet stream, surface heating anomaly, atmospheric transient eddy anomaly

1. Introduction

It is evident from the observation that, within the wintertime westerly jet stream circumnavigating the globe in the upper-troposphere, there exist three westerly jet cores: the jet core over the ocean to the south of Japan Island, and two others over Saudi Arabia-Egypt and the east coast of the United States, respectively (Krishnamurti, 1961). The westerly jet stream spanning over East Asia and the West Pacific, with its jet core over the ocean to the south of Japan Island, has been considered as an important atmospheric circulation system connected with the weather and climate in the East Asian and Pacific regions (Ye et al., 1958; Zhu et al., 1990; Yang et al., 2002). It is shown that the largest interannual variability of the westerly jet stream over East Asia and the West Pacific is concentrated on the Pacific Ocean, but not over the Asian landmass (Yang et al., 2002). Therefore, the present study of jet stream anomaly and related study are focused over the East Asian coastal water-Pacific regions. The name of the West Pacific jet stream (WPJS; Cressman, 1981) is used to echo with the analysis domain.

The WPJS anomaly is also one of the key links among climate variations over the mid-latitude North Pacific. It is strongly related to the climate anomaly in China (Sun and He, 2004; Jhun and Lee, 2004). According to the climate dynamics, the mid-latitude climate variations are closely related to two types of forcing: the external atmospheric forcing such as sea surface temperature (SST) anomalies and/or land surface processes taking place in certain regions, and the internal dynamic processes operating within the atmosphere itself such as synoptic-scale transient eddy (STE) or blocking in the mid-high Pacific

*Supported by the National Natural Science Foundation of China under Grant Nos. 40675041, 40333026, and 40425009.
†Corresponding author: renxuej@nju.edu.cn.

and Atlantic Oceans (Hoskins and Pearce, 1983). The investigation related with the external forcing is well addressed. For example, in the tropical Pacific, the atmospheric circulation is influenced by the tropical SST anomalies through a local, thermally direct change in the circulation. Such anomalous signals in the tropical atmospheric circulation can have a considerable effect on the mid-high latitude circulation via "atmospheric bridge", leading to the mid-latitude atmospheric anomaly (Alexander et al., 2002; Zhou et al., 2002). Meanwhile, the maintenance and variation of the mid-latitude atmospheric circulation have a close conjunction with the thermal condition in the mid-latitude ocean (Zhao and McBean, 1996; Bo, 2002). For example, the influence of the heating anomaly in the Kuroshio region on the atmospheric circulation proceeds by changing the gradients of the atmospheric temperature and geopotential height between the mid and high latitudes (Zhao and McBean, 1996).

Up to now, the dynamical mechanism related to the wintertime climate anomaly in the mid-latitude North Pacific is still half-baked knowledge, because of the poor understanding of the internal transient eddy forcing associated with STE to the mid-latitude atmospheric anomaly in wintertime, compared with a much clearer image of the external forcing mentioned above (Wu and Wang, 1997; Geng and Huang, 1996; Kushnr et al., 2002; Ferreira and Frankignoul, 2005). Different with that in the tropical and high latitudes, the air-sea system in the mid-latitude demonstrates its unique features of oceanfront such as the Kuroshio current in the North Pacific and the Gulf Stream in the North Atlantic. In addition, the robust mid-latitude baroclinicity, characterized by the large meridional air-temperature gradient and corresponding vertical wind shear, leads to the occurrence of abundant STE activities zonally spanning over the mid-latitude ocean (Blackmon, 1976). Investigations have shown that such synoptic-scale activities gain available potential energy from large-scale time-mean flow and transform it into supporting the eddy development. On the other hand, the anomaly of the STE activities influences the time-mean flow through anomalous fluxes of heat and momentum, demonstrating a forcing effect on the mean flow (Geng and Huang, 1996; Hoskins et al., 1983; Lau, 1988; Lau and Nath, 1991). Recent studies suggest that transient eddy activities represented by STE have a symbiotic relationship with the atmospheric mean flow anomaly. They never appear independently and show close linkage with the atmospheric teleconnections (Zhu and Sun, 2000; Nakamura et al., 2002; Carillo et al., 2000; Sheng et al., 1998). These investigations depict a close correlation between transient eddy forcing anomaly and mid-latitude climate variations.

As an important member among the mid-latitude atmospheric circulations, the year-to-year variation of the WPJS location and intensity is necessarily linked with the oceanic heating anomaly. Meanwhile, the simultaneous STE anomaly also shows a crucial role in the WPJS anomaly via transient eddy thermal and dynamical forcing. Based on these considerations, our aim is to investigate the thermal and dynamical connections of WPJS anomalies with the oceanic thermal condition represented by the ocean surface sensible and latent heat fluxes, and with the internal transient eddy represented by STE over the Pacific sector in winter, in the hope of a much clearer view of the contribution of the transient eddy forcing represented by STE to the wintertime WPJS variations.

2. Dataset and methods

The atmospheric dataset for the analysis is from ECMWF (European Centre for Medium-range Weather Forecasts) reanalysis daily and monthly mean datasets named ERA-40, with a spatial resolution of $2.5° \times 2.5°$ in longitude and latitude and a period from September 1957 to August 2002. The 97-yr (1903-1999) SST data come from the Global Ice Sea Surface Temperature Dataset (GISST) provided by the British Meteorological Office with a spatial resolution of $1° \times 1°$. The paper takes the SST data of 43-yr from 1957 to 1999 for the calculation of the meridional SST gradient (MSG) in Fig.1a. The SST cannot represent well the heat transfer between air and ocean. Therefore, the sensible and latent heat fluxes from ERA-40 and NCEP/NCAR (National Centers for Environmental Prediction/National Center for Atmospheric

Research) are both used to represent the oceanic thermal condition in the Pacific. Some comparisons related with these two datasets are addressed in the paper. The wintertime is defined as the mean of December-January-February (DJF).

According to the band-pass-filtered technique based on Murakami (1979), the transient fluctuations associated with migratory synoptic-scale disturbances with a 2.5-6-day period have been extracted from the ERA-40 daily dataset. The STE activity in certain regions for an individual wintertime is measured as the DJF mean $\overline{v'^2}$ of 2.5-6-day band-pass-filtered data at 200 hPa. It is noticed that the STE activities are located zonally over the North Pacific and North Atlantic Oceans, coinciding with the regions of the cyclone/anticyclone activities. These regions are referred to as storm tracks (Blackmon, 1976).

The horizontal Eliassen-Palm vector ($\boldsymbol{E}$), defined as $\boldsymbol{E} = (\overline{v'^2 - u'^2}, -\overline{u'v'})$, is also calculated at 200-hPa level in this study. Hoskins et al. (1983) underlined that the divergence (convergence) of $\boldsymbol{E}$ corresponds to a forcing to the mean horizontal circulation via increasing (decreasing) the westerly mean flow. Therefore, it is a good indicator to measure the effectiveness of the STE forcing to the mean flow. Another approach to describe the dynamical interaction between STE and the time-mean flow is to investigate the sign and magnitude of local barotropic energy conversions between the time-mean flow and the perturbation field (Simmons et al., 1983; Black and Dole, 2000). The local barotropic energy conversion is directly proportional to the dot product of $\boldsymbol{E}$ and the horizontal gradient of the time-mean zonal wind: $\boldsymbol{E} \cdot \nabla \overline{u}$. A physical interpretation is that positive (negative) energy conversions occur when $\boldsymbol{E}$ is directed up (down) the gradient of $\overline{u}$, thereby acting to reduce (increase) spatial inhomogeneities in the field through barotropic momentum conversions from the zonal-mean flow (eddies) into the eddies (zonal-mean flow).

The parameters u and v denote the zonal and meridional wind. An overbar denotes a DJF time-mean flow and a prime indicates a perturbation. The EOF, linear regression and correlation technique are also used in this study.

3. Results

3.1 The spatial match-pattern between the North Pacific STE and mid-latitude air-sea system

Figure 1 shows the spatial distributions of the climatological mean wintertime STE represented by 200-hPa $\overline{v'^2}$, the corresponding $\boldsymbol{E}$, and $\boldsymbol{E} \cdot \nabla \overline{u}$ over the North Pacific, respectively. The climatological wintertime MSG and the 200-hPa zonal wind (u_{200}) are also depicted in Fig.1. The MSG is defined as the SST difference between two adjoining latitudes with the same longitude. A clear image of the climatological features of the North Pacific STE activities is exhibited in Fig.1. It is shown in Fig.1a that the fan-like STE activities span from the East Asian coastal water, where the maximal MSG occurs, to the mid-latitude Pacific past the date line, and gain the local maximal near the jet exit region. In Fig.1b, the maximal $\boldsymbol{E}$ region scatters eastward from the westerly jet center to the west coasts of North America. The vectors mainly direct eastward or southeastward. The energy conversion in Fig.1c is congruent with the distribution of $\boldsymbol{E}$ in Fig.1b. It displays a positive process in the jet entrance while a negative one in the jet exit region, which effectively increasing westerly wind near the jet core. From above, it demonstrates that there exists a close local match-pattern between STE and the mid-latitude Pacific air-sea system in winter.

3.2 Analysis of the wintertime 200-hPa WPJS variations

The EOF analysis is performed to the wintertime u_{200} anomalies over 0°-65°N, 100°-240°E in 1957-2001. The variances of the first three modes are 38%, 22%, and 14%, respectively, contributing more than 70% of the total variance. This suggests that the three modes can describe the most variations of WPJS. The spatial patterns of the first three EOF leading modes of the WPJS, and their corresponding time coefficients

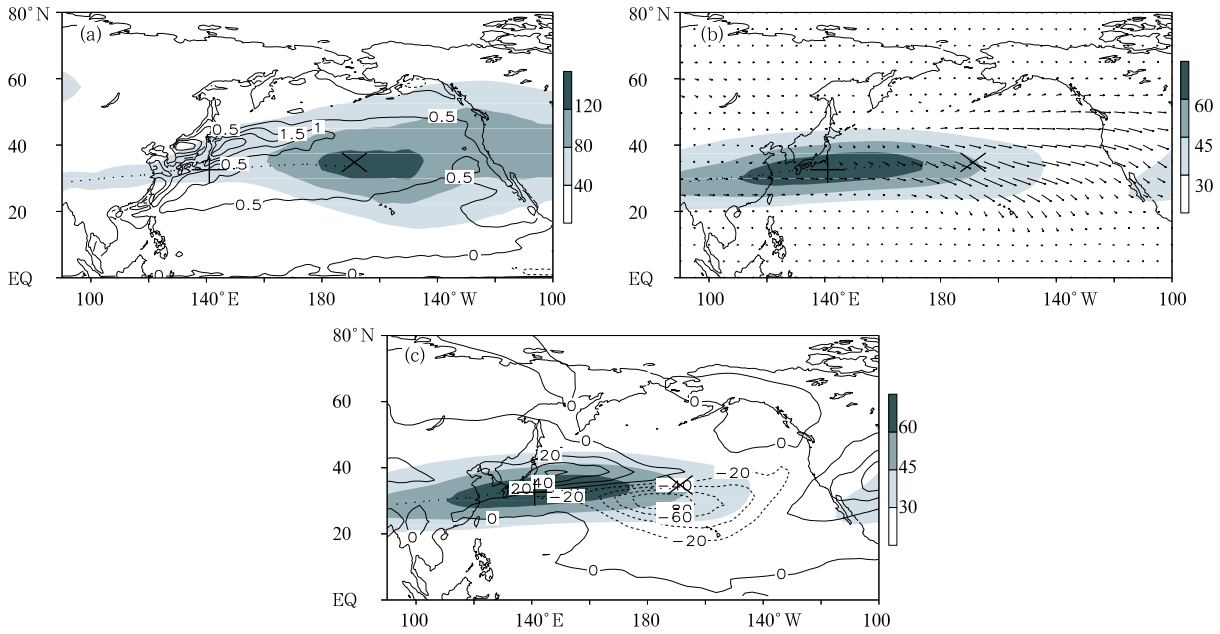

Fig.1. The climatological distributions of (a) the meridional SST gradient (contour, unit: K latitude^{-1}) and the STE at 200 hPa (shaded, unit: m^2 s^{-2}), (b) the zonal wind (shaded, unit: m s^{-1}) and $\boldsymbol{E}$ (units: m^2 s^{-2}) at 200 hPa, and (c) the zonal wind and $\boldsymbol{E}\cdot\nabla\overline{u}$ (contour, multiplied by 10^{-5}, units: m^2 s^{-3}) at 200 hPa over the North Pacific in winter. The axis and center of westerly jet stream and $\overline{v'^2}$ are indicated by the dotted line, + and ×, respectively.

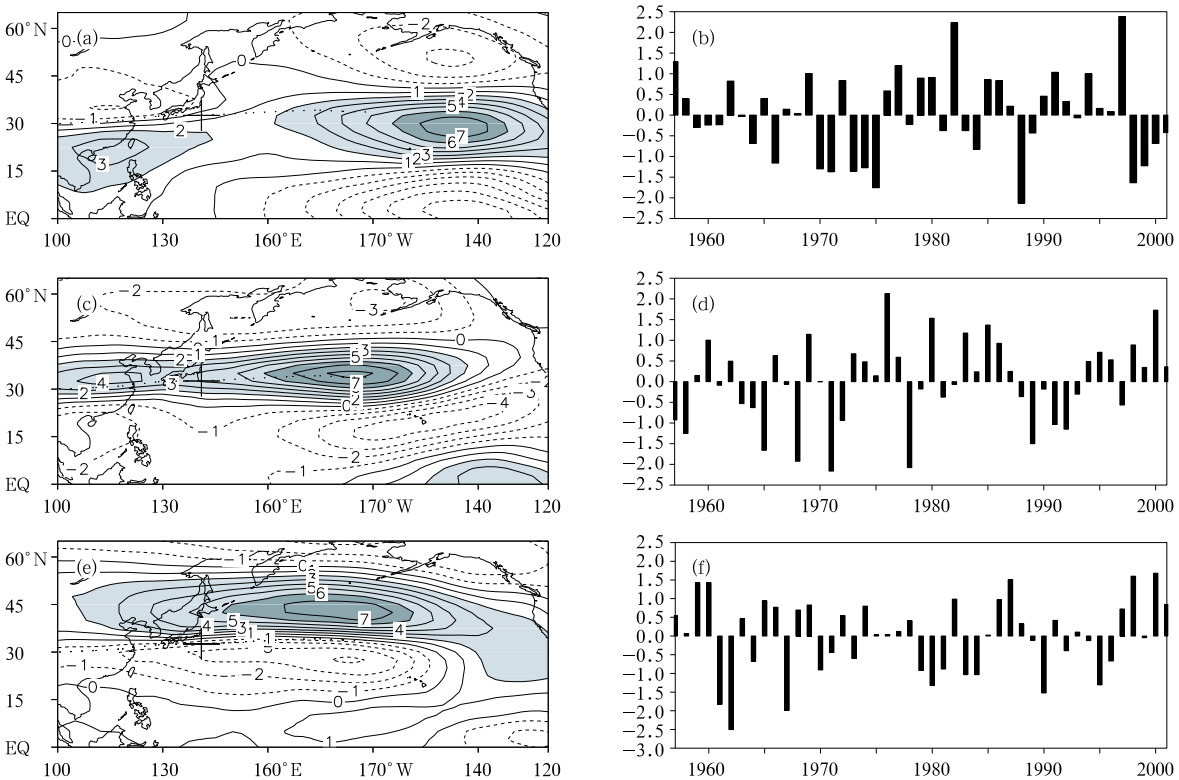

Fig.2. The spatial patterns (a, c, and e) and time coefficients (b, d, and f) of the first three EOF leading modes of the zonal wind at 200 hPa. The value in (a, c, and e) is multiplied by 100. The time coefficients are measured in units of their respective standard deviation.

measured in units of their respective standard deviation (denoted as PC1, PC2, and PC3, respectively), are plotted in Fig.2.

The first spatial pattern of the zonal wind anomaly (Fig.2a) shows a wave train of "−+−" pattern spanning from the tropical to mid-high latitude past the date line. The westerly wind anomaly in the mid-latitude mainly occurs over the Pacific past the date line. Meanwhile, a weak "−+−" dipolar anomaly exists over East Asia and its coastal water regions. However, the anomaly does not appear within the major part of the WPJS. The second spatial pattern (Fig.2c) shows the strengthened/weakened and flattened/widened westerly wind belt within WPJS main body. The third mode occupies more than 10% of the total variance, suggesting the statistical meaning to a certain extent. It shows the northward/southward-shift pattern of the wintertime WPJS and its corresponding time evolution (Figs.2e and f).

It is evident from Fig.2 that the anomalous patterns demonstrating the variations of the WPJS main body are the second and third EOF modes, namely, the strengthened/weakened WPJS and the northward/southward-shift WPJS. As discussed above, the first mode exhibits the strengthened/weakened westerly wind downstream of the WPJS main body.

3.3 Associations of wintertime WPJS anomalies with oceanic surface heating

In Figs.3-5 there are the patterns of regression of the wintertime surface latent and sensible heat fluxes against the normalized PC1, PC2, and PC3, respectively. It suggests the variability of the latent and sensible heat at the individual grid corresponding to a standard deviation of the time coefficients. For convenient comparison, the regression of u_{200} is also plotted in Figs.3-5. Values with magnitude larger than 95% confidence level are shaded. The regressed anomalies in Figs.3a and b, corresponding to the latent and sensible heat, respectively, are concentrated in two oceanic regions: the tropical center-eastern Pacific and the center of the North Pacific basin. Meanwhile, the latent heat anomaly dominates over the sensible heat flux. Though the results from NCEP/NCAR are similar to those from ERA-40, small discrepancy appears in the regressed sensible heat field. For example, significant region of sensible heat from ERA-40 is larger than that from NCEP/NCAR. It is confirmed that the strengthened/weakened wintertime westerly wind downstream of the WPJS main body in the upper-troposphere is strongly related to ENSO events (Yang et al., 2002; Matthews and Kiladis, 1999), via the significant changes of the convection over the tropical region and consequently changed atmospheric circulations over the mid-low latitudes (Matthews and Kiladis, 1999). Therefore, Fig.3 demonstrates the wintertime anomalous patterns of oceanic surface heating and WPJS associated with ENSO cycle. It depicts that accompanied with anomalous heat fluxes from oceans to the atmosphere in the tropical center-eastern Pacific and the center of the North Pacific basin, the upper-troposphere circulation anomalies present an enhanced subtropical westerly wind downstream of the WPJS main body and decreased zonal winds on its south and north sides.

Figure 4 shows the patterns of regression against PC2 that depicts the strengthened/weakened westerly wind belt within WPJS main body, especially in the eastern part of the jet axis near the jet exit region (Fig.4e). It is noted that the enhanced/reduced latent and sensible heat fluxes appear in the East Asian coastal water and the Kuroshio Current region, indicating more/less heat fluxes from oceans to the atmosphere in these regions, compared with the climatology. Meanwhile, a narrow area with decreased/increased heat fluxes extends from the west coasts of North America to the southeast side of the Kuroshio Current. The regressed latent heat still dominates sensible heat flux, compared Fig.4a with Fig.4b. The similar close relationship between the surface heat flux anomalies in the Kuroshio Current region and the strengthened/weakened westerly wind belt within WPJS main body is also shown in Figs. 4c and d from NCEP/NCAR dataset. However, the anomalous amplitude of the latent heat from NCEP/NCAR is slightly larger than that from ERA-40.

Figures 5a and b show the patterns of regression

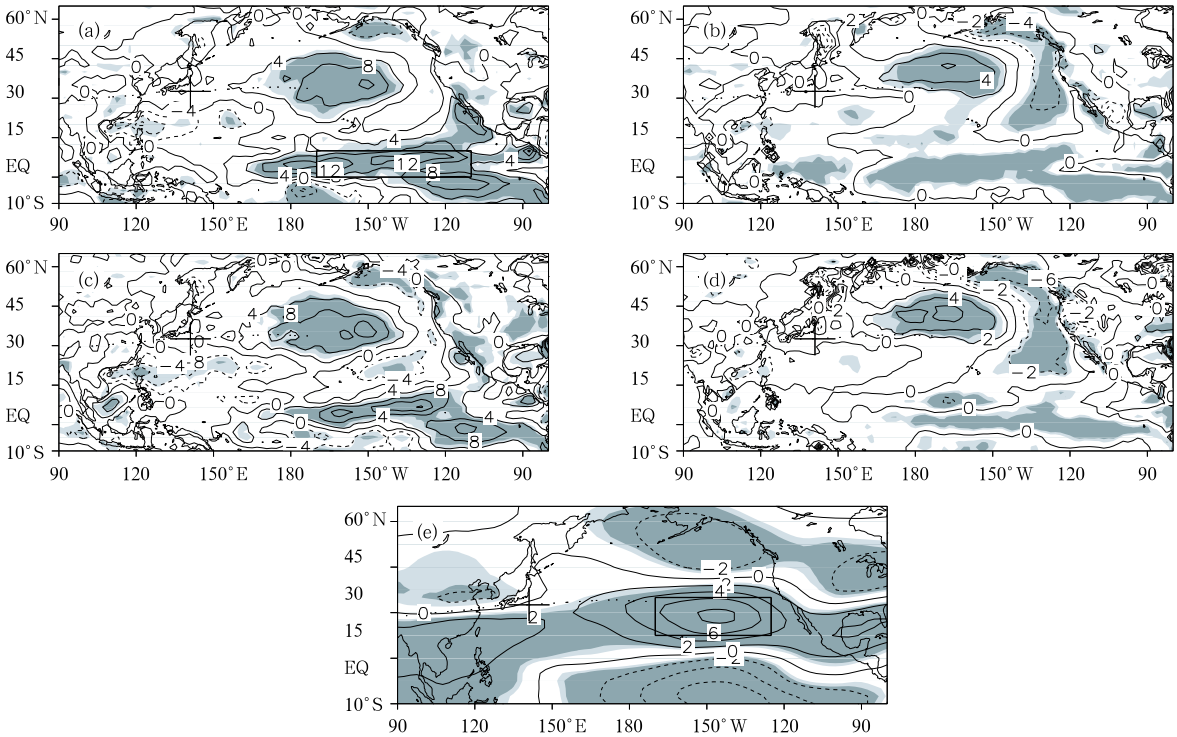

Fig.3. Regressions of PC1 on (a, c) the surface latent heat, (b, d) sensible heat, and (e) the zonal wind at 200 hPa. (a) and (b) for ERA-40, (c) and (d) for NCEP/NCAR, respectively. Values with magnitude larger than 95% and 99% confidence level are shaded with shallow and dark, respectively.

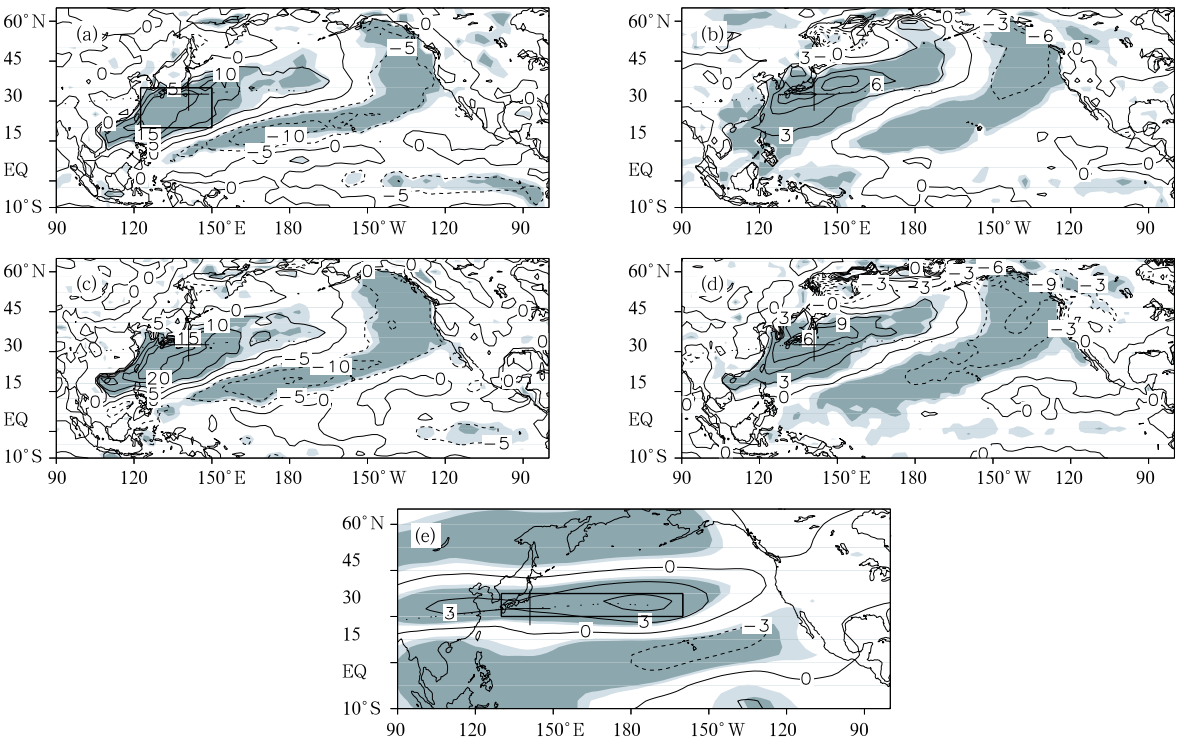

Fig.4. As in Fig.3, but for PC2.

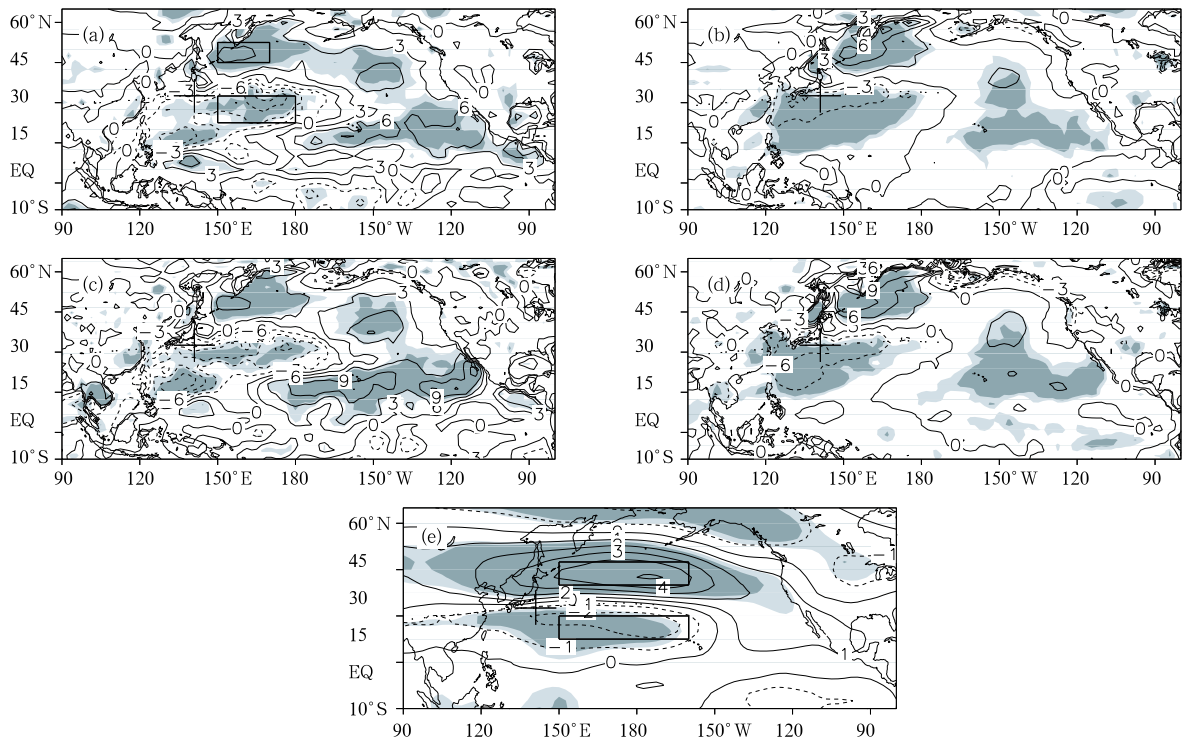

Fig.5. As in Fig.3, but for PC3.

of the wintertime surface heat fluxes against PC3. It is evident that a south-north dipolar pattern of surface heat fluxes, dominated between Kuroshio-to-its extension region and the poleward side of 35°N, is related with the northward/southward-shift pattern of WPJS. In addition, an increased/decreased heat flux occurs in the extratropical ocean past the date line. The regressed fields in Figs.5c and d from NCEP/NCAR dataset are still similar to those from ERA-40, however, a few anomalous regions from NCEP/NCAR also scatter in the South China Sea.

Do the coupled patterns between the wintertime WPJS variations and the surface heating anomalies in the North Pacific depicted above exist in reality? How about the coupled features of their time evolutions? Therefore, the key regions for WPJS and surface heating anomalies are obtained according to Figs. 3-5. The WPJS and surface heating indices are calculated based on the area-averaged zonal wind and surface heating over the key regions, to show the coupled features of their time evolutions. The key regions of the WPJS are chosen according to the significantly anomalous regions of the first three EOF spatial patterns. For the first and second modes, the key regions are 22.5°-35°N, 200°-235°E and 30°-37.5°N, 130°-200°E, respectively, framed in Figs.3e and 4e. The normalized time series of the area-averaged u_{200} over these two regions are used to represent the WPJS indices of PC1 and PC2, respectively. The WPJS third mode is slightly complicated due to the northward/southward-shift of the WPJS. Therefore, the normalized time series of the difference between the area-averaged zonal wind over north area (40°-47.5°N, 150°-200°E) and south area (22.5°-30°N, 150°-200°E) are used to represent the WPJS index of the third mode. Similarly, the key regions of the surface heating are also chosen according to the significantly anomalous regions of the regressed fields shown in Figs.3-5. For the first and second modes, they are 0°-10°N, 190°-250°E and 20°-35°N, 122.5°-150°E, respectively. For the third mode, the north and south areas are 45°-52.5°N, 150°-170°E and 22.5°-32.5°N, 150°-180°E, respectively. Due to the similarity of the regressed latent and sensible heat flux patterns, above surface heating indices indicate the total of latent and sensible heat fluxes.

Figure 6 shows the time series of the WPJS and

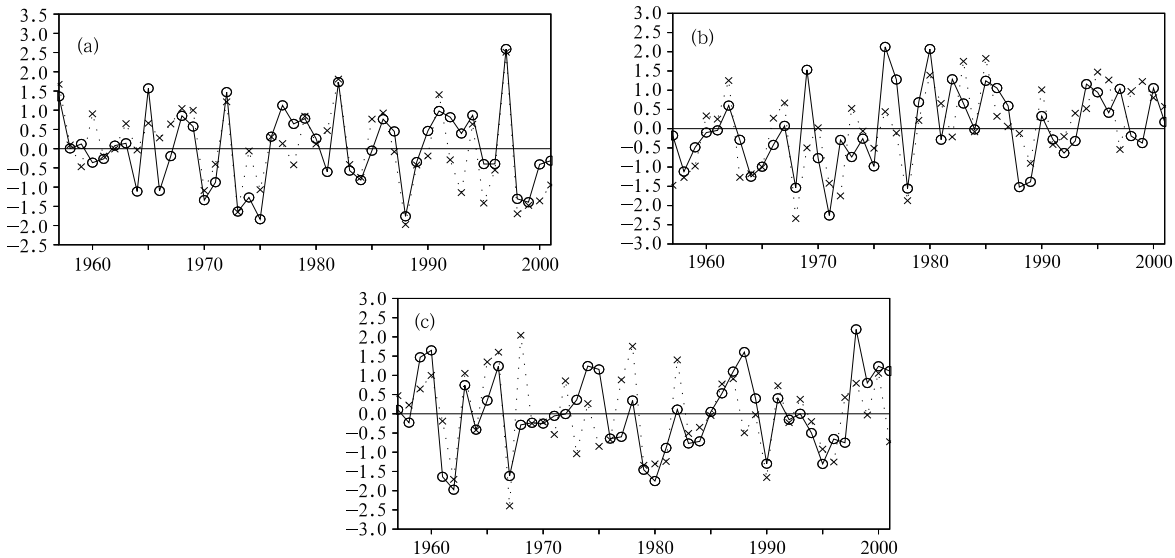

Fig.6. The time series of 200-hPa zonal wind index (circle line) and surface heating index (cross line). (a), (b), and (c) are corresponding to the indices of the first, second, and third modes of the 200-hPa zonal wind EOF, respectively. The areas for constructing the indices are shown as the frames in Figs.3-5.

surface heating indices of the three modes mentioned above. The correlation coefficients are 0.77, 0.60, and 0.58 for the three groups, respectively, indicating a congruent evolution on interannual time scales between wintertime WPJS variations and surface heating anomalies in the North Pacific key regions. In addition, the evolutions of three surface heating indices constructed from the NCEP/NCAR dataset are largely consistent with those from ERA-40 above, as can be inferred from the high correlation coefficients of 0.84, 0.98, and 0.96 between the three heating indices, and those from the NCEP/NCAR dataset for the corresponding three EOF modes, respectively. The discrepant surface heating anomalies between the two datasets mainly exist in the central-eastern Pacific before 1966.

3.4 Associations of wintertime WPJS anomalies with STE

Similarly, the patterns of regression of $\overline{v'^2}$, $\boldsymbol{E}$, and barotropic energy conversion $\boldsymbol{E}\cdot\nabla\overline{u}$ related with STE against PC1, PC2, and PC3 are displayed in Figs.7-9, respectively. It is noted in Fig.7 that the increased westerly wind over the mid-east Pacific past the date line is accompanied by the significantly intensified STE activities around the south-southeast of the increased westerly wind area. The corresponding regressed $\boldsymbol{E}$ directs eastward, northeastward, and southeastward scattering from the center of the anomalous westerly wind, leading to the acceleration effect to the local westerly wind. Meanwhile, Fig.7c exhibits enhanced barotropic energy conversion from STE to the time-mean westerly wind exhibited by the large negative value, and thus to speed up the local westerly wind. It is evident that the intensified STE activities over the mid-east Pacific past the date line show direct dynamic forcing effect on the increased local westerly wind, inferred from the view of the Eliassen-Palm and barotropic energy conversion between the STE and time-mean flow.

In Fig.8, the regressed STE against PC2 is dominated by the intensified STE activities in the eastern part of the jet stream, especially near the jet exit region, accompanied by the reduced STE activities poleward side of the WPJS. The corresponding regressed $\boldsymbol{E}$ directs eastward and northeastward scattering from the center of the anomalous westerly wind. Meanwhile, the large negative barotropic energy conversion anomaly appears in the same region. Both indicate the dynamic forcing effect of the anomalous STE

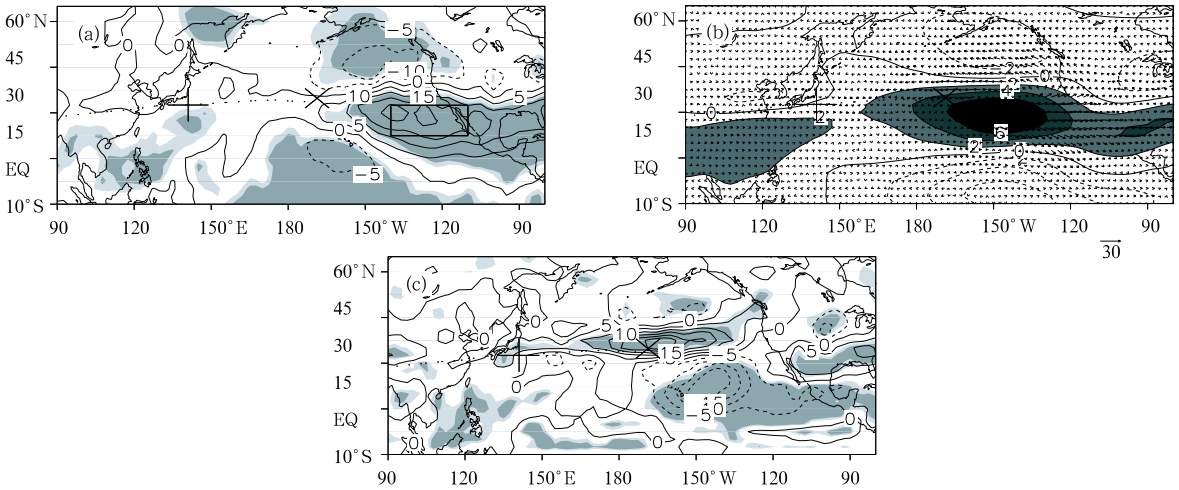

Fig.7. Regressions of PC1 on (a) the STE $\overline{v'^2}$, (b) $\boldsymbol{E}$, and (c) $\boldsymbol{E}\cdot\nabla\overline{u}$ at 200-hPa level. Values with magnitude larger than 95% and 99% confidence level are shaded with shallow and dark, respectively. Contour in (b) is regression of PC1 on 200-hPa zonal wind.

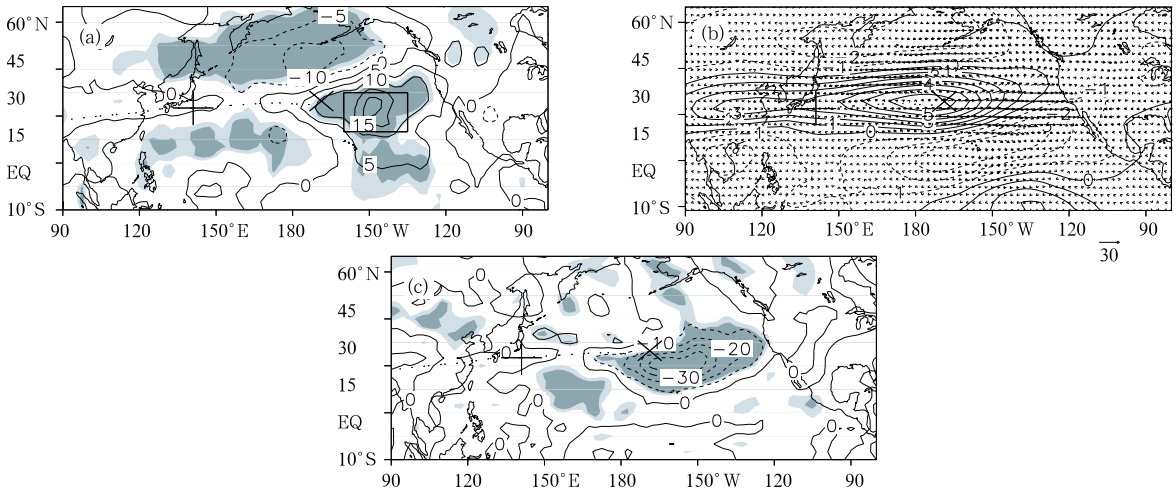

Fig.8. As in Fig.7, but for PC2.

activities on the increased westerly wind in the eastern part of jet stream. The regressed patterns of $\overline{v'^2}$, $\boldsymbol{E}$, and $\boldsymbol{E}\cdot\nabla\overline{u}$ against PC3 in Fig.9 display the anomalous distributions of the STE activities associated with the northward/southward-shift of the jet stream. In Fig.9, the STE spatial displacement is in conjunction with jet stream shifts in the same direction. When the jet stream shifts northward as shown in Fig.9b, the STE is also more active poleward side of the jet stream, accompanied by the eastward and southeastward $\boldsymbol{E}$ scattering from the positive center of the anomalous westerly wind north side of the climatological jet axis, and more negative barotropic energy conversion located in a narrow area spanning from the jet axis center to the jet exit. Above distributions of the anomalous STE reinforce the northward shift of the WPJS.

Similar to Fig.6, the STE indices, denoted as STEI1, STEI2, and STEI3, are constructed by averaging the 200-hPa $\overline{v'^2}$ in the regions boxed in Figs.7a, 8a, and 9a, respectively. The time evolutions of the three STE indices and the three WPJS indices defined in Section 3.3 are depicted in Fig.10. The correlation coefficients are 0.68, 0.72, and 0.64 for the three groups, indicating a strong linkage between the three leading

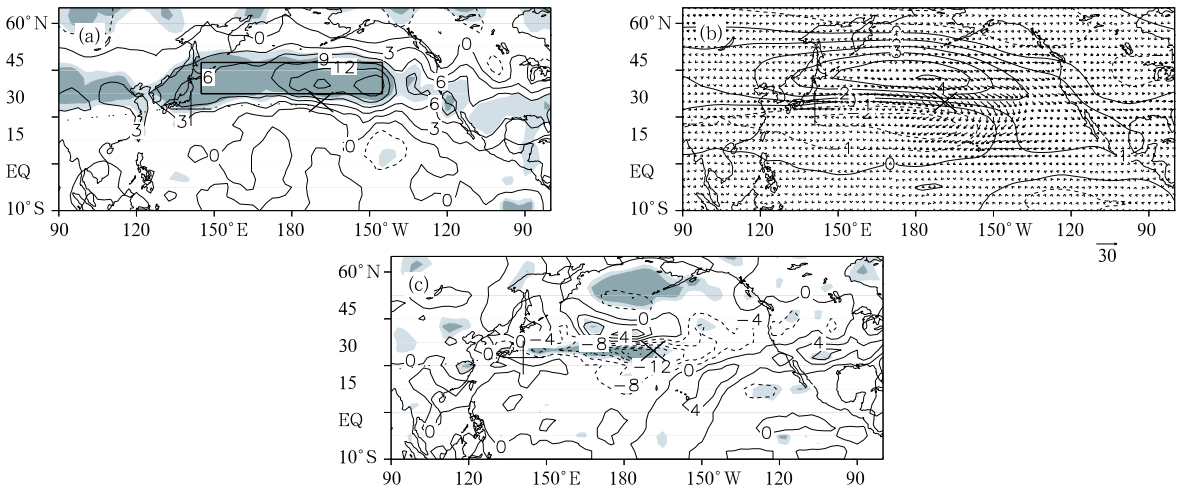

Fig.9. As in Fig.7, but for PC3.

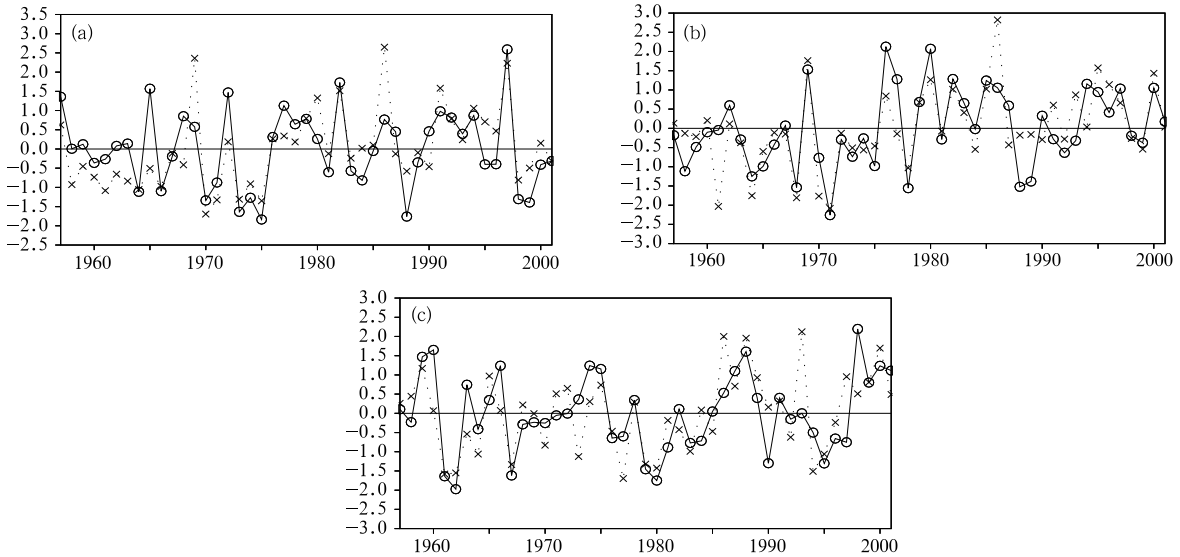

Fig.10. As in Fig.6, but for the time series of WPJS index (circle line) and STE index (cross line) at 200 hPa. The areas for constructing the STE indices are shown as the frames in Figs.7-9.

modes of the WPJS variations and STE anomalies over the mid-latitude North Pacific in winter.

3.5 Discussion about the coupled relationship among oceanic surface heating, STE, and WPJS anomalies in winter

Above addressed the relationship between wintertime WPJS, oceanic surface heating anomalies, and STE anomalies. In fact, previous studies have suggested that they are inseparable in the mid-latitude Pacific region, and construct a triangular coupled relationship (Ren et al., 2007). Namely, the changed atmospheric circulation associated with the changes of oceanic thermal condition induces the anomaly of the mid-latitude baroclinicity, and thus leading to the STE anomaly. The changed STE activities then have a forcing effect on the atmospheric circulation through the internal atmospheric dynamical and thermal processes. Therefore, the wintertime anomalous pattern of the mid-latitude atmospheric circulation is the final equilibrium state generated by both the external forcing and internal atmospheric forcing. Actually, the

first EOF spatial mode of the WPJS is the anomalous atmospheric circulation forced by ENSO (Yang et al., 2002; Matthews and Kiladis, 1999). The present study demonstrates further that the strengthened/weakened STE activities, induced directly by the strengthened/weakened atmospheric baroclinicity in the extratropical mid-east Pacific past the date line during the ENSO years (figure omitted), can directly yield the increased/decreased local westerly wind via the internal dynamics. Therefore, it can reinforce the westerly wind anomaly forced by ENSO. For the second mode, the increased/decreased oceanic surface heating in the East Asian coastal water and Kuroshio Current region is closely related to the increased/decreased meridional air-temperature contrast overhead, and with consequently inducing the strengthened/weakened WPJS in the upper-level through thermal wind relationship. Meanwhile, the strengthened/weakened atmospheric baroclinicity on the south side of the WPJS (figure omitted) causes the increased/decreased STE activities, which has a direct dynamic forcing to the increased/decreased local westerly wind in the eastern part of WPJS. For the third mode, the south-north dipolar pattern of the oceanic surface heating anomaly in the Northwest Pacific may shift the maximal region of the meridional air-temperature gradient northward/southward, inducing the northward/southward shift of the WPJS and STE simultaneously. The northward/southward shift of the STE is in favor of the WPJS northward/southward shift. Some of the results are in agreement with Zhu and Sun's (2000) investigations.

In fact, STE anomaly also plays a role in the time-mean air-temperature via thermal forcing, therefore, indirectly generating wind field anomaly. This issue will be discussed in another study.

4. Conclusions

Up to now, it is recognized that the dynamical process, related with the wintertime mid-latitude climate anomaly in the Northern Hemisphere, is not so easy to be understood as that suggested by linear theory (Hoskins and Karoly, 1981). Besides considering the direct forcing of diabatic heating, the active wintertime STE and its dynamic forcing to the climate anomaly in the mid-latitude, which is the considerable difference with that in the low-latitude, should be addressed necessarily. The latter belongs to the internal atmospheric processes (Kushnr et al., 2002). Therefore, it is essential to compare the effects of the two forcings on the mid-latitude climate anomaly, in order to assess the potential contribution of the STE forcing to the development of the mid-latitude climate anomaly. Based on these thoughts, the present study addresses the connections of WPJS anomalies with the oceanic surface sensible and latent heat fluxes, and with STE over the Pacific sector in winter. The following conclusions are obtained:

(1) The regressed analysis displays that the oceanic surface heating anomalies in the Pacific accompanied with WPJS three different anomalous patterns are discrepant. The anomalous westerly wind downstream of the WPJS main body is associated with the anomalous surface heating occurring in the tropical central-eastern Pacific past the date line and the center of the North Pacific basin. The fluctuation of westerly wind intensity in the WPJS region is strongly related with the surface heating anomaly in the Kuroshio Current region. The WPJS northward/southward-shift has a connection with south-north dipolar pattern of the heating anomaly in the western North Pacific separated at 35°N.

(2) The STE anomalous patterns, appearing over the extratropical central-eastern Pacific, the wintertime WPJS jet exit region and the north/south side of the climatological jet axis, are corresponding to WPJS three different anomalous patterns, respectively. The STE anomaly can directly generate the westerly wind anomaly through internal atmospheric process.

(3) There exists a triangular coupled relationship among wintertime oceanic surface heating anomaly, STE anomaly, and WPJS anomaly. The heating anomaly has a linkage with the time-mean flow and change the mid-latitude baroclinicity, leading to the STE anomaly. The changed STE activities then reinforce the WPJS anomaly through the internal dynamical processes.

It should be pointed out that the wintertime WPJS variation is not only related to the oceanic surface heating anomaly, but also due to the direct land thermal and dynamical processes such as Eurasian

orography (Wu et al., 2005) and East Asian snow cover (Martyn and Serreze, 2000). In the present study, only the oceanic surface heating in the North Pacific is demonstrated as the presentation of the external forcing. Therefore, the relationship between these persistent external forcings and WPJS should be investigated comprehensively. Furthermore, the related numerical simulation and dynamical analysis should be carried out in the future study.

REFERENCES

Alexander, M. A., B. Ileana, M. Newman, et al., 2002: The atmospheric bridge: The influence of ENSO teleconnections on air-sea interaction over the global oceans. *J. Climate*, **15**, 2205-2231.

Blackmon, M. L., 1976: A climatological spectral study of the 500-mb geopotential height of the Northern Hemisphere. *J. Atmos. Sci.*, **33**, 1607-1623.

Black, R. X., and R. M. Dole, 2000: Storm track and barotropic deformation in climate model. *J. Climate*, **13**, 2712-2728.

Bo Qiu, 2002: The Kuroshio extension system: Its large-scale variability and role in the mid-latitude ocean-atmosphere interaction. *J. Oceanography*, **58**, 57-75.

Carillo, A. et al., 2000: Storm tracks and zonal mean flow variability: A comparison between observed and simulated data. *Climate Dyn.*, **16**, 219-228.

Cressman, G. P., 1981: Circulations of the west Pacific jet stream. *Mon. Wea. Rev.*, **109**, 2450-2463.

Ferreira, D., and C. Frankignoul, 2005: The transient atmospheric response to mid-latitude SST anomalies. *J. Climate*, **18**, 1049-1067.

Geng Quanzhen and Huang Ronghui, 1996: The forcing of anomalous divergent wind and transient vorticity fluxes to the anomaly of stationary waves. *Acta Meteor. Sinica*, **54**(2), 132-141. (in Chinese)

Hoskins, B. J., and D. J. Karoly, 1981: The steady and linear response of a spherical atmosphere to thermal and orographic forcing. *J. Atmos. Sci.*, **38**, 1179-1196.

Hoskins, B., and R. Pearce, 1983: *Large-scale Dynamical Processes in the Atmosphere*. Academic Press, London, 111-112.

Hoskins, B. J., I. N. James, and G. H. White, 1983: The shape, propagation and mean-flow interaction of large-scale weather systems. *J. Atmos. Sci.*, **40**(7), 1595-1612.

Jhun, J. -G., and E. -J. Lee, 2004: A new East Asian winter monsoon index and associated characteristics of the winter monsoon. *J. Climate*, **17**, 711-726.

Krishnamurti, T. N., 1961: The subtropical jet stream of winter. *J. Meteor.*, **18**, 172-191.

Kushnr, Y. et al., 2002: Atmospheric GCM response to extratropical SST anomalies: Synthesis and evaluation. *J. Climate*, **15**, 2233-2256.

Lau, N. -C., 1988: Variability of the observed midlatitude storm tracks in relation to low-frequency changes in the circulation pattern. *J. Atmos. Sci.*, **45**, 2718-2743.

Lau, N. -C., and M. J. Nath, 1991: Variability of the baroclinic and barotropic transient eddy forcing associated with monthly changes in the mid-latitude storm track. *J. Atmos. Sci.*, **48**, 2589-2613.

Matthews, A. J., and G. N. Kiladis, 1999: Interactions between ENSO, transient circulation, and tropical convection over the Pacific. *J. Climate*, **12**, 3062-3086.

Martyn, P. C., and M. C. Serreze, 2000: Effects of variations in East Asian snow cover on modulating atmospheric circulation over the North Pacific Ocean. *J. Climate*, **13**, 3700-3710.

Murakami, M., 1979: Large-scale aspects of deep convective activity over the GATE area. *Mon. Wea. Rev.*, **107**, 994-1013.

Nakamura, H. et al., 2002: Interannual and decadal modulations recently observed in the Pacific storm track activity and East Asian winter monsoon. *J. Climate*, **15**, 1855-1874.

Ren Xuejuan, Yang Xiuqun, and Han Bo, 2007: Leading coupled modes between the atmosphere and ocean in the North Pacific in winter and their association with the transient eddy anomalies. *Acta Meteor. Sinica*, **65**(1), 52-62. (in Chinese)

Sheng, J., J. Derome, and M. Klasa, 1998: The role of transient disturbance in the dynamics of the Pacific-North American pattern. *J. Climate*, **11**, 523-536.

Simmons, A. J., J. M. Wallace, and G. Branstator, 1983: Barotropic wave propagation and instability and atmospheric teleconnection patterns. *J. Atmos. Sci.*, **40**, 1363-1392.

Sun Linhai and He Min, 2004: The relationship between summer precipitation in China and circulation anomaly in Euroasia and its application in precipitation prediction. *Acta Meteor. Sinica*, **62**(3), 355-364. (in Chinese)

Wu Guoxiong and Wang Jingfang, 1997: Correlation in middle and high latitudes between winter sea surface temperature and 500-hPa geopotential height. *Acta Meteor. Sinica*, **55**(1), 11-21. (in Chinese)

Wu Guoxiong, Wang Jun, Liu Xin, et al., 2005: Numerical modeling of the influence on Eurasian orography on the atmospheric circulation in different seasons. *Acta Meteor. Sinica*, **63**(5), 603-612. (in Chinese)

Yang S., K. -M. Lau, and K. -M. Kim, 2002: Variation of the East Asian jet stream and Asian-Pacific-American winter climate anomalies. *J. Climate*, **15**, 306-325.

Ye Duzheng, Tao Shiyan, and Li Maicun, 1958: The abrupt changes of the atmospheric circulation in June and October. *Acta Meteor. Sinica*, **29**(4), 249 -263. (in Chinese)

Zhao Yongping and G. A. McBean, 1996: Influence of the Kuroshio region marine heating anomaly on the North Hemisphere atmospheric circulation in the following seasons. *Oceanologia ET Limnologia Sinia*, **27**(3), 246-250.

Zhou Tianjun, Yu Rucong, and Li Zhaoxin, 2002: ENSO-dependent and ENSO-independent variability over the mid-latitude North Pacific: Observation and air-sea coupled model simulation. *Adv. Atmos. Sci.*, **19**, 1127-1147.

Zhu Baozhen, Ding Yihui, and Luo Huibang, 1990: A review of the atmospheric general circulation and monsoon in East Asia. *Acta Meteor. Sinica*, **48**(1), 4-16. (in Chinese)

Zhu Weijun and Sun Zhaobo, 2000: Interannual variability of northern winter Pacific storm track and its association with 500-hPa height and tropical and Northern Pacific sea surface temperature. *Acta Meteor. Sinica*, **58**(3), 309-320. (in Chinese)